Research Article

ADVANCED PHOTONICS

Superresolution imaging using superoscillatory diffractive neural networks

Hang Chen,[a,†] Sheng Gao,[a,†] Haiou Zhang,[a,†] Zejia Zhao,[a] Zhengyang Duan,[a] Gordon Wetzstein,[b] and Xing Lin[a,c,*]

[a]Tsinghua University, Department of Electronic Engineering, Beijing, China
[b]Stanford University, Department of Electrical Engineering, California, United States
[c]Tsinghua University, Beijing National Research Center for Information Science and Technology, Beijing, China

Abstract. Optical superoscillation enables far-field superresolution imaging beyond diffraction limits. However, existing superoscillatory lenses for spatial superresolution imaging systems still confront critical performance limitations due to the lack of advanced design methods and limited design degree of freedom. Here, we propose an optical superoscillatory diffractive neural network (SODNN) that achieves spatial superresolution for imaging beyond the diffraction limit with superior optical performance. SODNN is constructed by utilizing diffractive layers for optical interconnections and imaging samples or biological sensors for nonlinearity. This modulates the incident optical field to create optical superoscillation effects in three-dimensional (3D) space and generate the superresolved focal spots. By optimizing diffractive layers with 3D optical field constraints under an incident wavelength size of λ, we achieved a superoscillatory optical spot and needle with a full width at half-maximum of 0.407λ at the far-field distance over 400λ without sidelobes over the field of view and with a long depth of field over 10λ. Furthermore, the SODNN implements a multiwavelength and multifocus spot array that effectively avoids chromatic aberrations, achieving comprehensive performance improvement that surpasses the trade-off among performance indicators of conventional superoscillatory lens design methods. Our research work will inspire the development of intelligent optical instruments to facilitate the applications of imaging, sensing, perception, etc.

Keywords: superresolution imaging; photonic neural networks; optical superoscillation.

Received Mar. 31, 2024; revised manuscript received Aug. 26, 2024; accepted for publication Sep. 10, 2024; published online Oct. 7, 2024.

[DOI: 10.1117/1.AP.6.5.056004]

1 Introduction

The Abbe–Rayleigh diffraction limit of traditional optical equipment has always been an obstacle to the study of micro- and nanoscale objects.[1,2] Near-field microscopic imaging techniques, such as contact photography[3] and scanning near-field imaging,[4,5] capture evanescent fields by placing a probe or light-sensitive material extremely close to the object to achieve nanoscale resolution, which is not possible for imaging inside biological samples or encapsulated micro- and nanostructures. Far-field microscopic imaging technology is not restricted by the above bottlenecks. Some typical far-field microscopic imaging techniques, such as single-molecule localization (SML) microscopy[6,7] or stimulated emission depletion (STED),[8,9] have demonstrated the possibility of nanoscale imaging without capturing evanescent fields. However, SML microscopy and STED typically require intense beams to excite, deplete, or bleach fluorophores in a sample that produces photobleaching and phototoxicity in living samples.

Optical superoscillations are rapid subwavelength spatial variations of light intensity and phase that occur in complex electromagnetic fields formed by the precise interference of coherent waves, which provide an advanced method for far-field superresolution imaging beyond the diffraction limit.[10,11] To generate optical superoscillation, complicated lens design methods[12–14] have been proposed. Additionally, Fresnel zone plate (FZP) optimization design methods, including optimizing

*Address all correspondence to Xing Lin, lin-x@tsinghua.edu.cn
†These authors contributed equally to this work.

algorithms[15–18] and optimization-free algorithms,[19,20] have also been developed. However, the existing superoscillatory focusing-based imaging designs require a trade-off among performance indicators and have limited performance as follows: (1) strong sidelobes resulting in a small field of view (FoV),[12,15,20] (2) short working distances,[13,15,16,19] (3) limited depth-of-focus (DoF),[15,17,18,21] and (4) chromatic aberration caused by wavelength-dependent phase retardation,[13,14,19,22] which dramatically limit their applications.

The performance limitations of the existing superoscillatory imaging methods are mainly due to the optimization with two-dimensional (2D) optical field constraints. These constraints include limited modulation element numbers or only ring-structured phase modulation, which substantially limits the degree of freedom in design space for optimizing performance. For example, the conventional superoscillatory lens design methods, such as the pinhole array mask[11] or FZPs,[17] require the following steps. First, the prolate ellipsoid function or Strehl ratio is used as the optimization function of the model. Then, the phase distribution of the superoscillatory lens is optimized with the constraints of full width at half-maximum (FWHM) of the superoscillatory spot $I_{(x_i,y_i)}$ at the 2D position of (x_i, y_i), and the sidelobe intensity $I_{\sum_{(x_j,y_j)}}$ at a combination of the 2D positions $\sum_{(x_j,y_j)}$ in the local FoV expressed by the distance r between the superoscillatory spot and sidelobes. The above optimization method can only achieve the design of a pinhole array mask with a limited element number or a simple FZP with the ring-structured phase modulation of 0 or 1, while the optimization process requires a very complex formula decomposition process.

Here, we propose constructing the superoscillatory diffraction neural networks, i.e., superoscillatory diffractive neural networks (SODNNs), that generate optical superoscillation in 3D and achieve superresolution imaging beyond the diffraction limits, as shown in Fig. 1(a). SODNN is constructed by utilizing diffractive layers to implement optical interconnections and imaging samples or biological sensors to implement nonlinearity. The conventional superoscillatory lens design methods usually optimize the 2D superoscillatory spot with sidelobes around the focus spot, as shown in Fig. 1(b). SODNN modulates the incident optical field to create optical superoscillation effects in 3D space and generates the superresolved focusing spots or optical superoscillatory needle, as shown in Fig. 1(c). The diffraction limit of existing photonic neural network systems is due to training neural networks without exploring the superoscillatory effects. By constructing the large-scale SODNN that optimizes the optical coefficients of a stack of diffractive layers to modulate the optical field in 3D space, we can generate superoscillation at any local regions without sidelobes across the FoV and with long working distance, long DoF, and achromatic spots for high-performance superresolution imaging.

2 Methods

The forward model of SODNN is based on angular spectrum representation. The complex-valued coherent input optical field U_{λ_k} at the wavelength λ_k $(k = 1, 2, \ldots, N)$ is transformed by SODNN before the detection. We consider the diffractive modulation layers of SODNN in this work with the complex transform function of $M_{\lambda_k}(\Delta H, z_i)$ that modulates the incident optical field to the output optical field at the plane with a distance of z_i. Here, ΔH represents the relative height map of the diffractive elements in SODNN to generate optical path difference and modulate the phase ϕ_{λ_k} of incident optical field, which can be formulated as $\Delta H = \lambda_k \phi_{\lambda k}/2\pi\Delta n_{\lambda_k}$ with Δn_{λ_k} being the wavelength-dependent material refractive index. Then, the output optical fields at the wavelength λ_k at the output plane with a distance of z_i can be formulated as $U'_{\lambda_k}(z_i) = M_{\lambda_k}(\Delta H, z_i)U_{\lambda_k}$, and the detector measures the intensity distribution of output optical fields that can be formulated as a nonlinear function such as the square of the complex optical field: $I_{\lambda_k}(z_i) = |U'_{\lambda_k}(z_i)|^2 = |M_{\lambda_k}(\Delta H, z_i)U_{\lambda_k}|^2$. We optimize the relative height of diffractive elements at different modulation layers with 3D optical field constraints across different wavelength channels. The optimization of large-scale diffractive elements reduces chromatic aberration caused by wavelength-dependent phase retardation, thereby enhancing the system's robustness to wavelength variations.[23] For the multiwavelength SODNN, the total intensity distribution of different wavelengths at the output plane can be formulated as the superposition of detected intensity distribution at each wavelength: $I(z_i) = \sum_{\lambda_k} I_{\lambda_k}(z_i)$.

The SODNN is optimized with the 3D optical field constraints, which optimizes the shape of the superoscillatory focusing spot within a certain distance range $z_i \in [f - \Delta f, f + \Delta f]$ before and after the focal plane with a focal length of f. The ideal superoscillatory focusing spot $I_{(x_i,y_i,z_i)}$ at a position in the 3D space with coordinates (x_i, y_i, z_i) at the output plane with a distance of z_i would have a maximized energy focused spot $I_{(x_i,y_i,z_i)}$ and minimized light intensity sidelobes $I_{\sum_j (x_j,y_j,z_i)}$ at a combination of position coordinates $\sum_j (x_j, y_j, z_i)$. Taking the ideal output light intensity as the optimization direction with the entire 3D optical field constraints, the SODNN performs the function of a neuromorphic photonic processor that utilizes weighted optical diffractive interconnections of massively diffractive neurons to achieve the desired optical superoscillatory function. In addition, we further design the constraint to maximize the energy transmission efficiency of superoscillatory regions by minimizing the optical energy outside the superoscillatory regions. Therefore, the 3D optical field constraint optimization of SODNN can be formulated as

$$\min_{\Delta H}\Bigg(\sum_{z_i\in[f-\Delta f, f+\Delta f]}(((I_{(x_i,y_i,z_i)} + I_{\sum_j (x_j,y_j,z_i)}) - I_{\text{target}})^2 + \text{MSE}(I_{(x,y,z)\notin(x_i,y_i,z_i)}))\Bigg), \tag{1}$$

where $I_{(x_i,y_i,z_i)}$ is the intensity of the superoscillatory focusing spot at the 3D position of (x_i, y_i, z_i); $I_{\sum_j (x_j,y_j,z_i)}$ is the intensity of the sidelobes at the 3D positions of $\sum_j (x_j, y_j, z_i)$; I_{target} is the ground-truth label that represents the ideal superoscillatory output; $\text{MSE}(I_{(x,y,z)\neq(x_i,y_i,z_i)})$ represents the total energy of optical intensity outside the superoscillatory regions with the mean square error (MSE) function; $z_i \in [f - \Delta f, f + \Delta f]$ is the range of the 3D optical field constraint optimization space before and after the focal plane with a focal length of f; and ΔH is the relative height map of the diffractive elements.

For the design of SODNN in this work, we use the stochastic gradient descent approach to optimize the network coefficients on a desktop computer (Linux) with an Intel Xeon Gold 6226R CPU at 2.90 GHz with 16 cores, and an NVIDIA GTX-3090Ti GPU with 24 GB graphics card memory. The residual error of network outputs with respect to ground-truth labels and the total

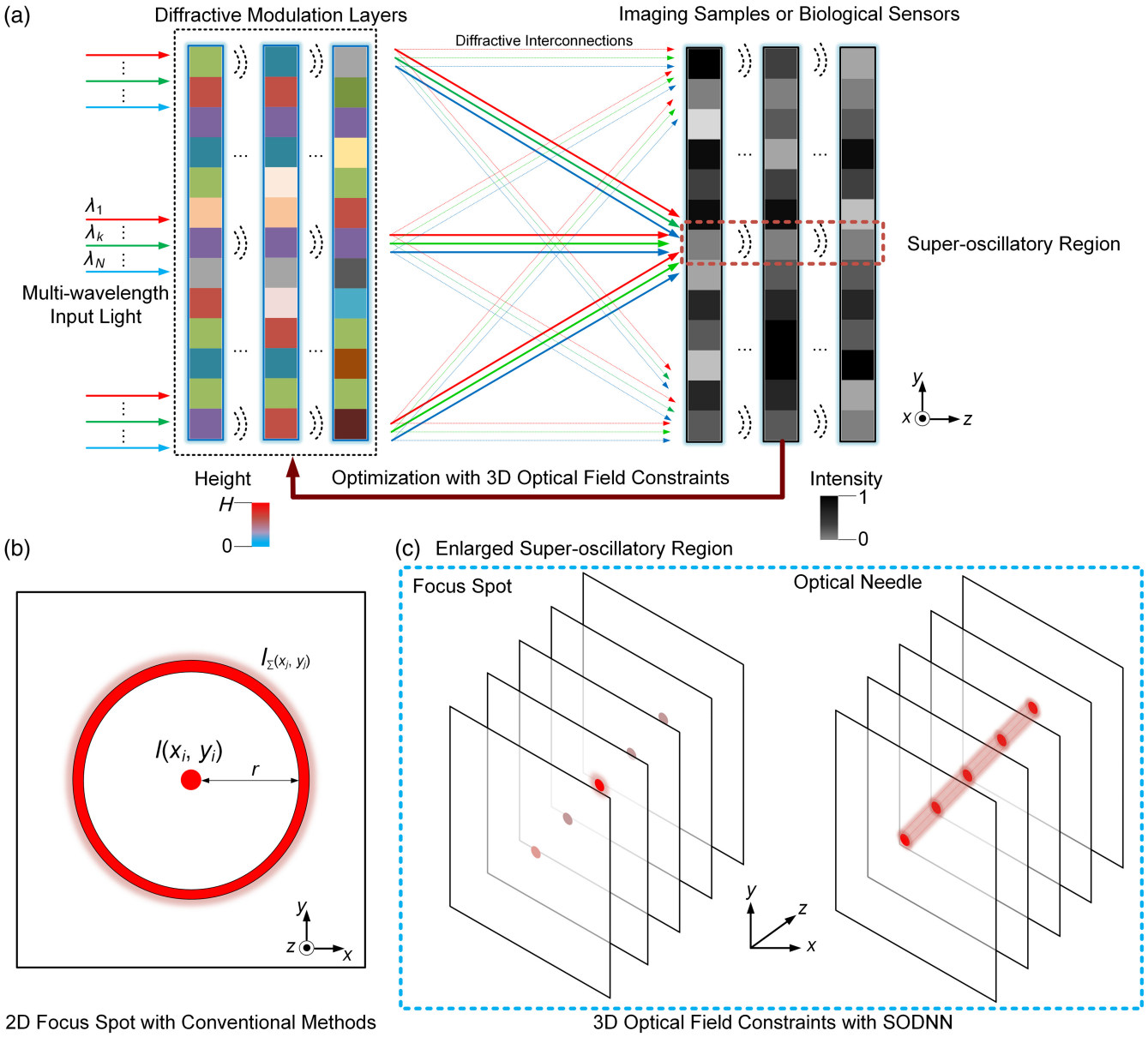

Fig. 1 Training SODNN to optimize the diffractive elements with 3D optical field constraints. (a) Utilizing diffractive modulation layers and free-space propagation to implement the weighted optical interconnections, and imaging samples or biological sensors to implement nonlinearity. SODNN can modulate the multiwavelength incident optical field to create optical superoscillation effects in 3D superoscillatory regions. (b) The conventional methods optimize a 2D focus spot at a specific focusing distance to achieve optical superoscillation with a large sidelobe. (c) The enlarged 3D superoscillatory regions show that SODNN optimizes the 3D optical field in a certain distance range to achieve superoscillation without the sidelobe.

optical energy outside the superoscillatory regions are calculated according to Eq. (1), which are used to perform the error backpropagation to optimize the SODNN and the relative height map ΔH of the diffractive modulation elements in SODNN.

3 Results

3.1 Numerical Evaluations

We first validate the effectiveness of the 3D optical field constraint optimization of SODNN in achieving superoscillatory spots without sidelobes to realize a large FoV at the designed long focal length f, as shown in Figs. 2(a) and 2(b). Each optical diffractive element size was set to $\lambda/2 \times \lambda/2$, where λ is the wavelength of input coherent light, which is 632.8 nm. We designed a one-layer SODNN with a modulation element number of 2500×2500, corresponding to a network layer size of 0.79 mm $\times$ 0.79 mm. The selection of the above parameters was determined according to the performance analysis of SODNN, as discussed in Sec. 4.2. The proposed system forms a superoscillatory focused spot with almost no sidelobes at a long focal length $f = 250\ \mu\text{m}\ (\sim 400\lambda)$, with an FWHM of

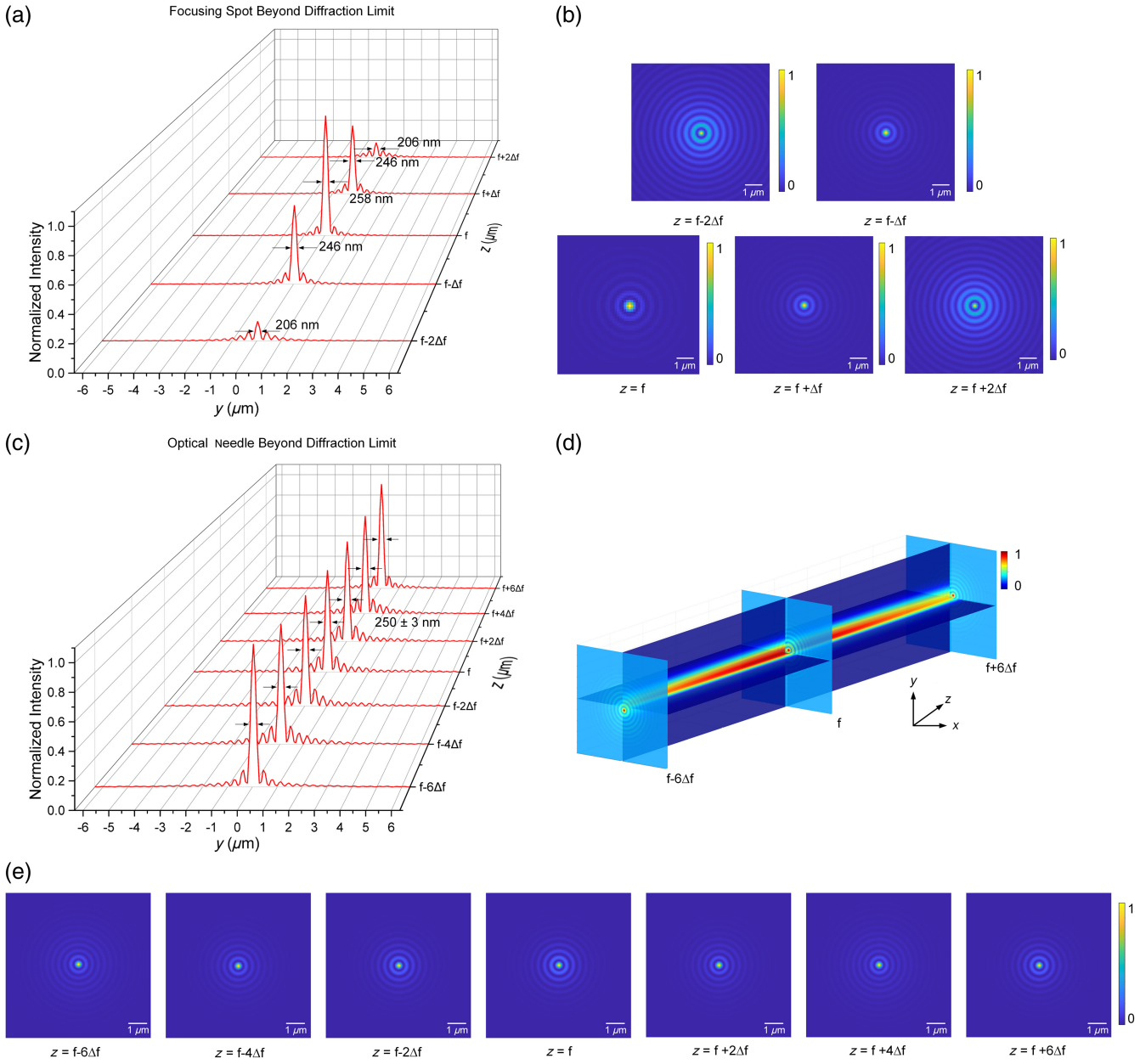

Fig. 2 Optical superoscillatory spots and optical needle design of SODNN. The FWHM (a) and the output (b) of superoscillatory spots at the designed focal length and distributions offsetting the designed focal length with the collimated input optical field. (c) The optical superoscillatory needle within a DoF of 6 μm with uniform light intensity and consistent FWHM. (d) The 3D distributions of the output optical superoscillatory needle. (e) The output of the slices of the optical superoscillatory needle.

258 nm [$\sim 0.407\lambda$; this is shown in the middle of Fig. 2(a) and the lower left of Fig. 2(b)]. Recent achievements of the superoscillatory lenses compared with SODNN are shown in Sec. 4.1, which demonstrates the extraordinary performance of SODNN.

It can be found that optimizing the SODNN only at a designed focal length f [that is $\Delta f = 0$ in Eq. (1)], SODNN can maintain the morphology of the superoscillatory focus spot and avoid the appearance of sidelobes at the designed position; once it exceeds this distance, the sidelobes will appear immediately accompanied by smaller FWHM and weaker superoscillatory focusing spot intensity. For example, at four different focal lengths $f - 2\Delta f$, $f - \Delta f$, $f + \Delta f$, and $f + 2\Delta f$ where $\Delta f = 0.25$ μm, we found that the sidelobes appeared and the FWHM was reduced to 206 nm ($\sim 0.325\lambda$), 246 nm ($\sim 0.388\lambda$), 246 nm ($\sim 0.388\lambda$), and 206 nm ($\sim 0.325\lambda$), respectively, as shown in Figs. 2(a) and 2(b). For the out-of-focal planes, the intensity of the sidelobes increases exponentially with respect to the central spot as the central spot size decreases, demonstrating the high quality of optical sectioning of the SODNN for imaging.

In order to maintain the profiles of superoscillatory light spots within a long DoF range, that is, to form a superoscillatory light needle, we optimize the shape of the superoscillatory

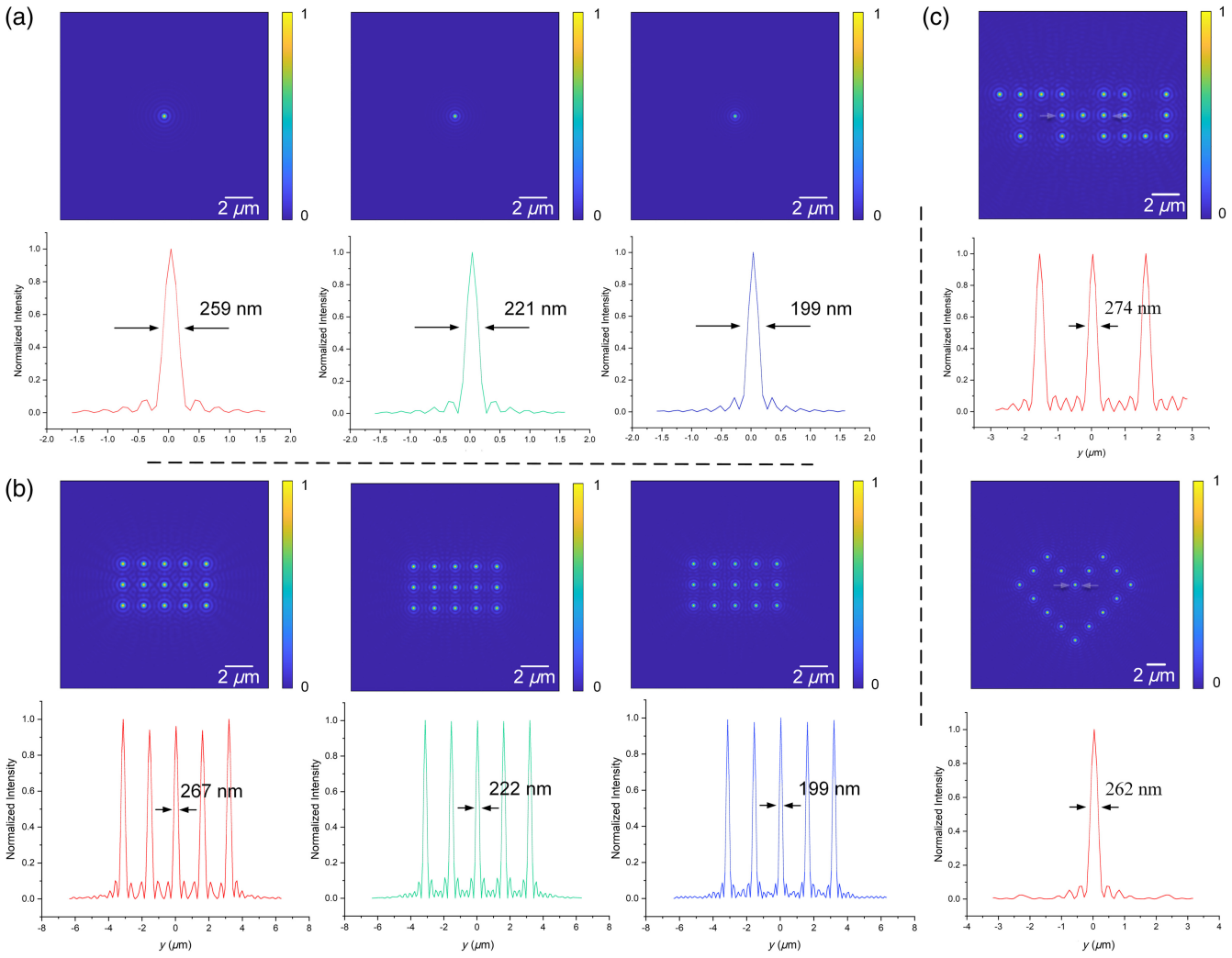

Fig. 3 Multiwavelength and multifocus SODNNs. (a) The superoscillatory spots under red, green, and blue light channels with the FWHM of 259, 221, and 199 nm, respectively. (b) The 3 × 5 superoscillatory spot arrays under red, green, and blue light channels with the FWHM of 267, 222, and 199 nm, respectively. (c) The superoscillatory spots of the T-H-U pattern with the FWHM of 274 nm and the superoscillatory spots of the heart-shaped pattern with the FWHM of 262 nm.

focusing spot within a certain distance range $[f-6\Delta f, f+6\Delta f]$ before and after the focal length f, as shown in Figs. 2(c)–2(e). Each optical diffractive element size was set to $\lambda/2\times\lambda/2$, where $\lambda = 632.8$ nm. We evaluate the performance of one-layer SODNN by setting the modulation element number to 1500×1500, corresponding to the network layer size of 0.47 mm × 0.47 mm. We set the range of the 3D optical field constraint optimization space $z_i \in [f-6\Delta f, f+6\Delta f]$, where $f = 100$ μm and $\Delta f = 0.5$ μm. We found that an optical superoscillatory needle was formed within a long DoF of 6 μm [$\sim10\lambda$, see Fig. 2(d)]. The optical superoscillatory needle was further tested by selecting seven positions in the range $[f-6\Delta f, f+6\Delta f]$ with $2\Delta f$ as the sampling interval [see the slices of the optical superoscillatory needle in Fig. 2(e) and the FWHM in Fig. 2(c)]. It can be found the optical superoscillatory needle has uniform light intensity and consistent FWHM (250 ± 3 nm) in the designed DoF.

Based on our earlier studies,[23,24] we further demonstrate the multiwavelength SODNN to solve the chromatic aberration problems caused by wavelength-dependent phase retardation, as shown in Figs. 3(a) and 3(b). In this design, three different parallel wavelength channels [i.e., blue, green, and red light with the wavelengths of 473 nm (λ_1), 532 nm (λ_2), and 632.8 nm (λ_3), respectively] are used to generate multiwavelength superoscillatory light spots focused at the same focal length. Each optical diffractive element size was set to $\lambda_3/2\times\lambda_3/2$. We also designed a one-layer SODNN by setting the modulation element number to 2500×2500, corresponding to the network layer size of 0.79 mm × 0.79 mm. The proposed system forms multiwavelength superoscillatory focused spots with almost no sidelobes at a long focal length $f = 250$ μm ($\sim400\lambda_3$), with the FWHM of 259, 221, and 199 nm, respectively, produced by red light, green light, and blue light, shown in Fig. 3(a), respectively. Using the integrated multifocus and multiwavelength design approach proposed above, we further design a multiwavelength multifocus SODNN, shown in Fig. 3(b), which can realize 3×5 superoscillatory focusing spot arrays under red, green, and blue light channels. The 3×5 superoscillatory focusing spot arrays were produced by red light, green light, and blue light with the FWHM of 267,

222, and 199 nm, respectively. The comparisons of the proposed SODNN with respect to the state-of-the-art achievements of superoscillatory designs are also discussed in Sec. 4.1. Some complex multifocus superoscillatory spots, such as heart-shaped pattern and T-H-U pattern (the abbreviation of Tsinghua University), are shown in Fig. 3(c) to demonstrate the superiority of SODNN in terms of design flexibility and versatility. For the above two multifocus arrays, we obtained the FWHM of 274 and 262 nm, respectively, beyond the diffraction limit ($0.61\lambda/\mathrm{NA} = 456$ nm).

3.2 Experimental Evaluations

We built the experimental setup to measure the SODNN's superoscillatory focusing spot profiles, as shown in Fig. 4(a). A He–Ne laser (25-STP-912-230, Melles Griot) with a wavelength of 632.8 nm and a power of 5 mW was collimated by lens 1 and lens 2, and a pinhole was used as a filter. The collimated He–Ne laser beam was used to illuminate the SODNN placed on the multi-axis translation stage (NPXYZ100SGV6, Newport), which was processed by two-photon printing technology (Moji Nano Technology, China). Considering the error accumulation and processing costs of large-scale devices in actual processing, we designed two kinds of small-scale one-layer SODNNs with the modulation element number of 200×200 corresponding to each optical diffractive element size of 500 nm × 500 nm and 1-bit step height of 0 and 500 nm to verify the correctness of SODNN. Figure 4(d) left and middle are, respectively, designed to achieve single-focus focusing and a 2×2 multifocus array focusing of superoscillatory spots, while Fig. 4(d) right is the enlarged part of the processed 2×2 multifocus SODNN after characterization by electron microscopy (EM). An Olympus objective (100× magnification, NA = 0.9) was used to image the light focused by the designed SODNNs. A tube lens with focal length $f = 180$ mm was used to form an image on a CMOS camera (01-MOMENT, Photometrics).

Figure 4(e) left and Fig. 4(f) left are the numerical analysis results of a single-focus superoscillatory focusing spot and 2×2 multifocus superoscillatory focusing spot array with a focal length $f = 20$ μm, at its design wavelength $\lambda = 632.8$ nm. The spot morphology is highly consistent with the experimental measurement results shown in Fig. 4(e) middle and Fig. 4(f) middle. For the single-focus superoscillatory focusing spot and the 2×2 multifocus superoscillatory focusing spot array, the FWHMs obtained by numerical analysis results are 307 nm [see Fig. 4(e) right] and 340 nm [see Fig. 4(f) right], respectively. However, due to the systematic errors during the optical processing, the experimentally measured FWHMs were 383 nm [see Fig. 4(e) right] and 392 nm [see Fig. 4(f) right], respectively. By utilizing an *in situ* training algorithm, e.g., adaptive training methods,[25,26] with the programmable diffractive layers, the system can adapt to a wide range of tuning errors, preserving performance during deployment. These strategies present a viable approach to enhance the robustness of SODNNs. Although there was a slight gap with the numerical results, the experimental results still exceeded the diffraction limit ($0.61\lambda/\mathrm{NA} = 415$ nm).

For imaging, we used a scanning mode with SODNN, where the signal used to reconstruct the image is taken from the central part of the CMOS camera. This imaging strategy is also commonly used in confocal microscopy.[27,28] The experimental equipment is shown in Fig. 4(a), where the commercial resolution testing chart [TC-RT01, Technology Manufacture, Germany; see Fig. 4(b)] is used as the target for measurement. The resolution testing chart's pattern structure is achieved by processing metallic chromium (Cr) on a glass substrate (S_iO_2) with the smallest line width of 0.152 μm. The 500-line pair pattern that cannot be clearly imaged by a commercial Olympus objective [see Fig. 4(b)] can be clearly imaged through SODNN [see Fig. 4(c)], demonstrating that SODNN has a performance comparable to the commercial microscopy imaging system. A more compact solution is to integrate SODNN with optical fiber to form an endoscope, as described in Sec. 4.4.

4 Discussion

4.1 Comparisons with State-of-the-Art Methods

Table 1 compares several typical performance indices of superoscillatory design with the proposed SODNN in this work. SODNN can achieve a long working distance with hundreds of micrometers, while the other works can only achieve a short working distance with only tens of micrometers. In terms of working distance, SODNN has achieved an improvement by an order of magnitude. SODNN can also achieve a DoF greater than 6 μm, and the ratio of FWHM to Rayleigh diffraction limit is less than 60%, which indicates its exceptional imaging capabilities and overall performance.

4.2 Performance Analysis of SODNN

We evaluate and compare the network performance under different modulation element numbers, i.e., $K \times K$, with $K = 100$, 200, 300, 500, 1000, and 2500 [Fig. 5(a)] when the number of layers is fixed at 1, and the diffractive element size is $\lambda/2 \times \lambda/2$. We also evaluate the network performance under different layer numbers when the modulation element numbers are fixed at 200×200 [Fig. 5(b)] and 300×300 [Fig. 5(c)] and the diffractive element size is $\lambda/2 \times \lambda/2$. We also analyze the effects of changes in neuron size, i.e., the diffractive element size was set to $\lambda/2 \times \lambda/2$, $\lambda \times \lambda$, $2\lambda \times 2\lambda$, and $4\lambda \times 4\lambda$ when the number of layers is fixed at 1 and modulation element number is 300×300 [see Fig. 5(d)]. We found that as the number of layers increases and the number of neurons in each layer increases, the FWHM of the superoscillatory spot without sidelobes will gradually become smaller and stabilize at $\sim 0.407\lambda$ [Figs. 5(a) and 5(c)]. It seems that the modulation element numbers have a greater impact than the layer numbers on the FWHM by comparing Figs. 5(b) and 5(c). When the modulation element numbers are small, no matter how the layer numbers increased, the FWHM of the superoscillatory spot without sidelobes cannot be stabilized at $\sim 0.407\lambda$. On the contrary, as the diffractive element size increases, the FWHM of the superoscillatory spot without sidelobes will gradually increase. The above results can guide system design, such that under specific system parameters, e.g., a one-layer SODNN with enough modulation element numbers, optimal performance comparable to a multilayer SODNN can be achieved, which thereby greatly reduces hardware complexity, system errors, and experimental difficulty and enhances robustness during system installation and adjustment.

4.3 Reconfigurable SODNN for Superoscillatory Spot Scanning

SODNN can modulate the incident optical field to create optical super oscillatory effects in any 3D space and generate

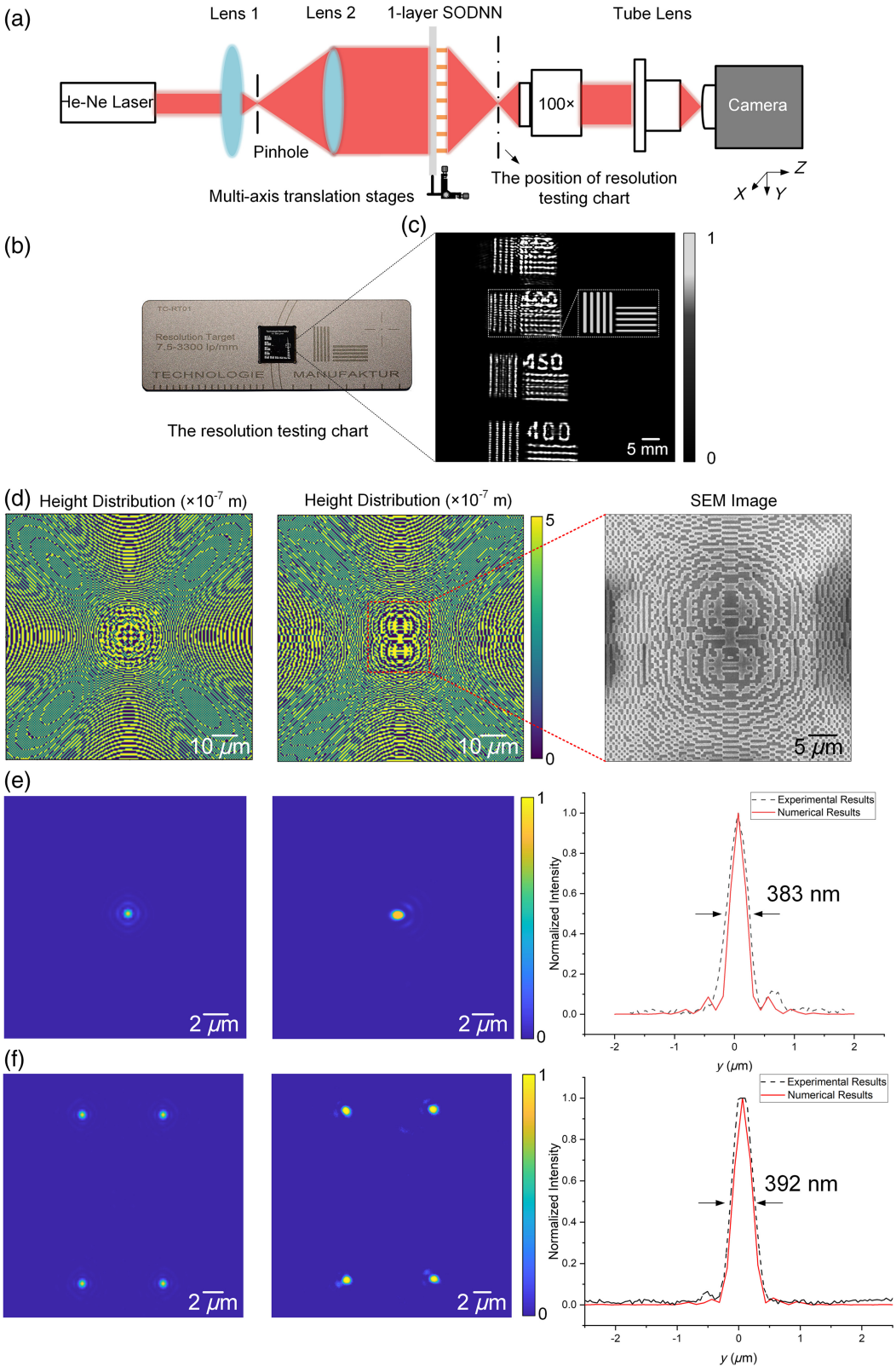

Fig. 4 Characterization of SODNN. (a) Schematic of the experimental setup. (b), (c) Imaging results of the resolution testing chart by commercial Olympus objective and SODNN. (d) The diffractive modulation layer of single-layer SODNNs for a single-focus (left) and 2×2 multifocus (middle) with the layer profile characterized by scanning electron microscope, i.e., SEM (right). (e) The numerical analysis results (left) and experimental results (middle) of the single-focus SODNN. (f) The numerical analysis results (left) and experimental results (middle) of the 2×2 multifocus SODNN.

Table 1 Comparisons of SODNNs with state-of-the-art superoscillatory methods.

Method	Wavelength (nm)	Focal length (μm)	DoF (μm)	FWHM (λ)	Ratio of FWHM/Rayleigh diffraction limit (0.61λ/NA)	Ambient medium	Refs.
Monochromatic superoscillatory design	640	10	—	0.289	64%	Oil	12
	810	10	—	0.45	85%	Air	20
	632.8	38	—	0.45	71%	Air	21
Achromatic superoscillatory design	405	—	—	0.457	67%	—	—
	532	10	—	0.445	65%	Air	17
	633	—	—	0.54	79%	—	—
Optical superoscillatory needle design	532	6	~5	0.34	81%	Oil	18
	405	55	~4.8	0.407	~65%	Air	22
Monochromatic superoscillatory design by SODNN	**632.8**	**250**	—	**0.407**	**57%**	**Air**	**This work**
Achromatic superoscillatory design by SODNN	**473**	—	—	**0.420**	**59%**	—	—
	532	**250**	—	**0.415**	**58%**	**Air**	**This work**
	632.8	—	—	**0.409**	**57%**	—	—
Optical superoscillatory needle design by SODNN	**632.8**	**100**	**6**	**0.395**	**60%**	**Air**	**This work**

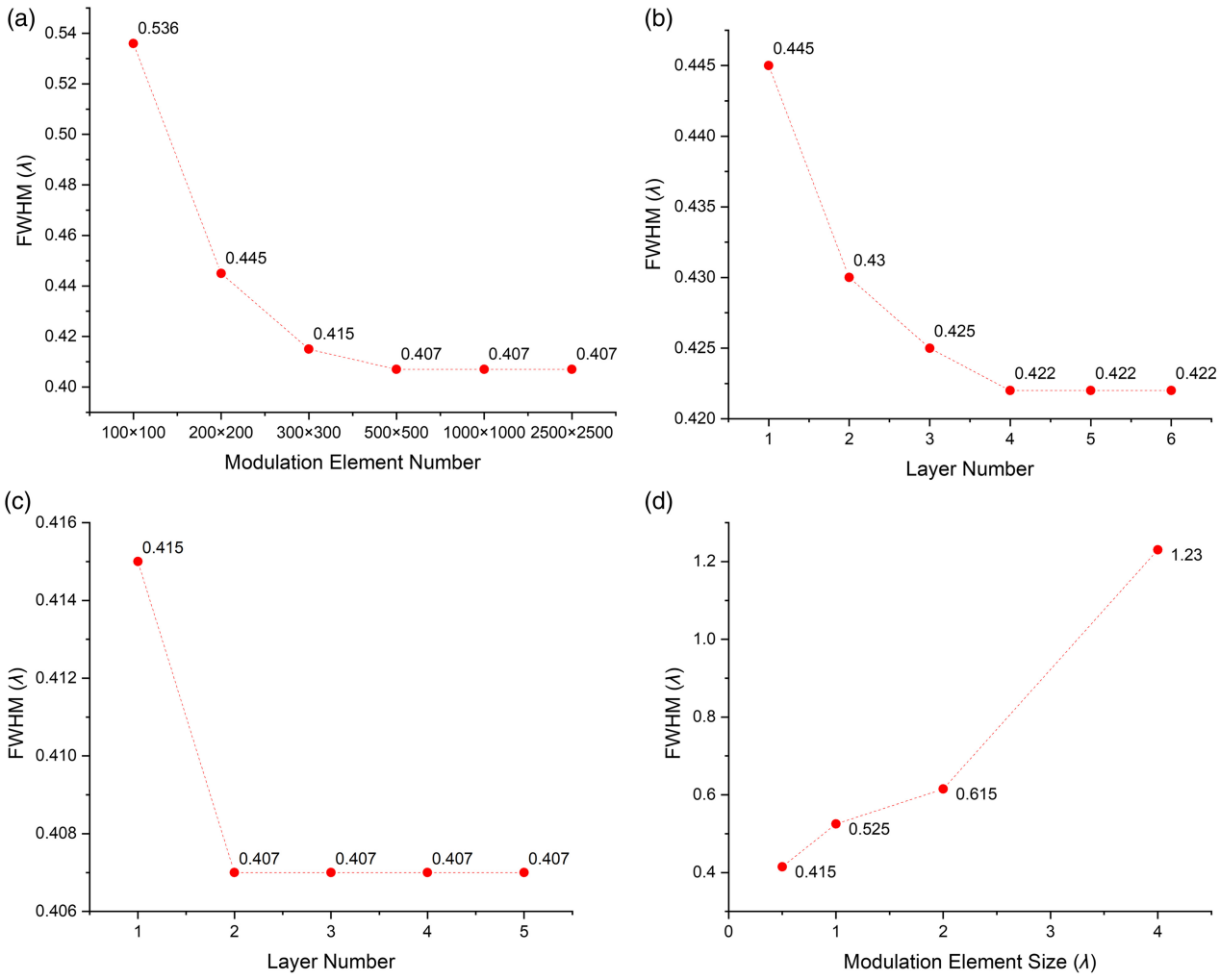

Fig. 5 Performance analysis of SODNN. The FWHM of the output spot with respect to the modulation element number (a), the layer number (b), (c), and the modulation element size (d).

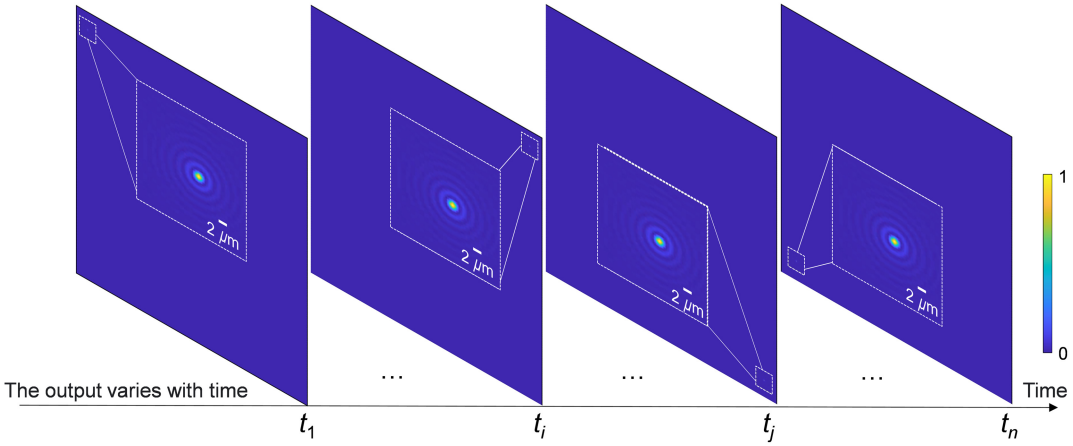

Fig. 6 Reconfigurable SODNN for superoscillatory imaging. The superoscillatory spot can raster scan over the field for imaging by dynamically programming the modulation coefficients of diffractive elements.

superresolved focusing spots. By training a series of SODNNs and loading them into a reconfigurable device such as a spatial light modulator (SLM), we can achieve dynamic scanning of superoscillatory spots. We designed a series of SODNNs by setting the modulation element number to 2500×2500 with the element size $\lambda/2 \times \lambda/2$ and $\lambda = 632.8$ nm, which corresponds to the network layer size of 0.79 mm $\times$ 0.79 mm with the focal length $f = 250$ μm. The FWHM remains at 258 nm ($\sim 0.407\lambda$) and does not change with the position of the superoscillatory spots. Figure 6 shows that SODNN can focus the superoscillatory spots at even the four most edge locations of the detection plane, which proves that SODNN can realize scanning at any position on the detection plane. Considering a high-speed SLM that works at 1000 frames per second and takes the

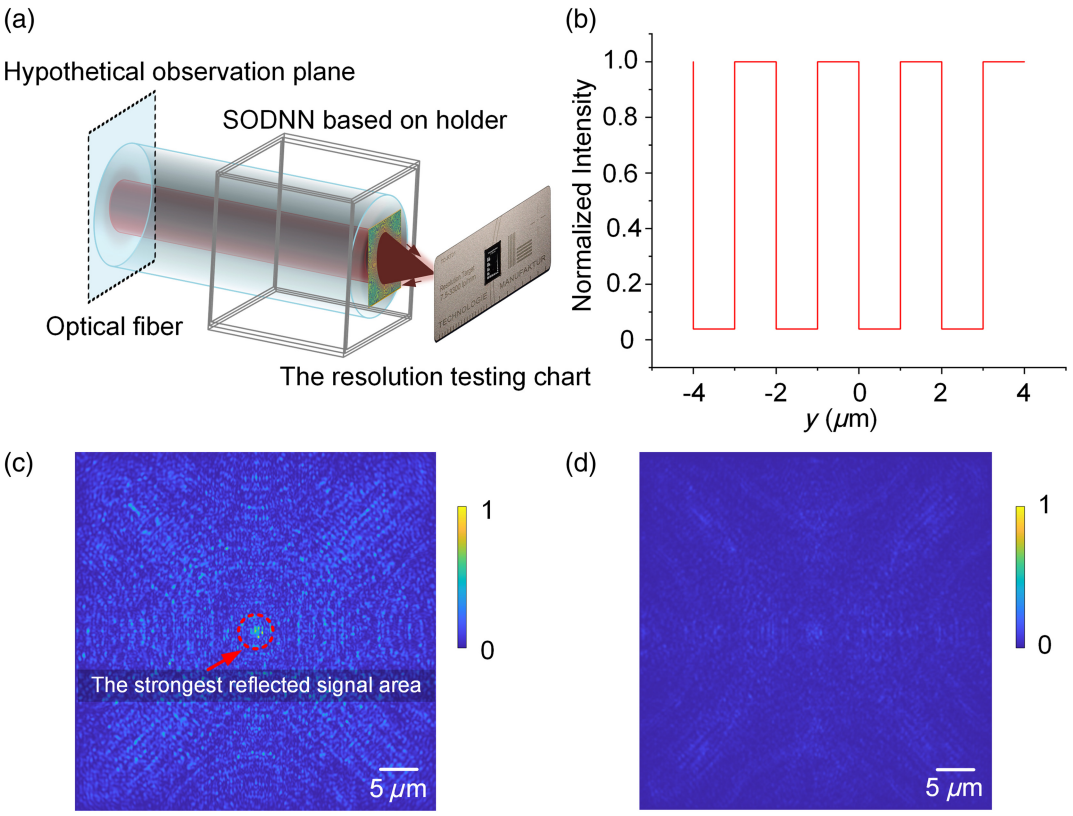

Fig. 7 Integrating SODNN with optical fiber. (a) Schematic diagram of the endoscope designed by integrating SODNN and optical fiber. (b) The imaging function is realized by utilizing the intensity of reflected light produced by different transmittance structures, such as the metal structure producing a strong reflection (c) and the glass forming a weak reflection on the hypothetical observation plane (d).

FWHM as the scanning interval, the SODNN can achieve a scanning range of 66.56 $\mu m^2/s$.

4.4 Integrating SODNN with Optical Fiber

A more compact solution is to integrate SODNN with optical fiber to form an endoscope, as shown in Fig. 7(a), and collect the reflection signal of the superoscillatory focusing spot from the measured target to complete the imaging process. By using Lumerical FDTD to arrange a hypothetical observation plane at the input end of SODNN to capture the topography of the reflected light field, we found the metal structure produces strong reflection [see Fig. 7(c)] with a normalized light intensity of 1; the glass forms a weak reflection with the normalized light intensity ~0 [see Fig. 7(d)]. Using the binary change of light intensity, we can also reconstruct the 500-line pair pattern of the measured resolution testing chart [see Fig. 7(b)].

5 Conclusion

We proposed SODNNs that demonstrate unparalleled advantages over other techniques for the realization of superoscillatory spots and imaging beyond the diffraction limit. SODNNs make it possible to flexibly design large FoV without sidelobes, long working distances, long DoF, and achromatic optical superoscillatory functions. SODNNs can work at any wavelength, from microwaves to ultraviolet waves,[29] which makes it possible to obtain superoscillatory spots with a smaller FWHM and further improve the resolution of SODNN imaging. We believe that this is a new cross-innovation in the fields of photonic neural networks, superresolution microscopy, and metasurfaces that will attract the attention of more scientists engaged in the development of intelligent optical instruments.[30–35]

Disclosures

The authors declare no competing interests.

Code and Data Availability

All relevant code is available from the corresponding author upon reasonable request.

Acknowledgments

This work was supported by the National Key Research and Development Program of China (Grant No. 2021ZD0109902), the National Natural Science Foundation of China (Grant No. 62275139), and the China Postdoctoral Science Foundation (Grant No. 2023M741889).

References

1. N. I. Zheludev, "What diffraction limit?" *Nat. Mater.* **7**(6), 420–422 (2008).
2. J. W. Goodman and P. Sutton, "Introduction to Fourier optics," *J. Eur. Opt. Soc. B* **8**(5), 1095 (1996).
3. E. Betzig and J. K. Trautman, "Near-field optics: microscopy, spectroscopy, and surface modification beyond the diffraction limit," *Science* **257**(5067), 189–195 (1992).
4. B. Hecht et al., "Scanning near-field optical microscopy with aperture probes: fundamentals and applications," *J. Chem. Phys.* **112**(18), 7761–7774 (2000).
5. J. A. Porto, R. Carminati, and J.-J. Greffet, "Theory of electromagnetic field imaging and spectroscopy in scanning near-field optical microscopy," *J. Appl. Phys.* **88**(8), 4845–4850 (2000).
6. M. Lelek et al., "Single-molecule localization microscopy," *Nat. Rev. Method. Primers* **1**(1), 39 (2021).
7. S. Colabrese et al., "Machine learning approach for single molecule localisation microscopy," *Biomed. Opt. Express* **9**(4), 1680–1691 (2018).
8. H. Blom and J. Widengren, "Stimulated emission depletion microscopy," *Chem. Rev.* **117**(11), 7377–7427 (2017).
9. J. N. Farahani, M. J. Schibler, and L. A. Bentolila, "Stimulated emission depletion (STED) microscopy: from theory to practice," *Microsc.: Sci. Technol. Appl. Educ.* **2**(4), 1539–1547 (2010).
10. N. I. Zheludev and G. Yuan, "Optical superoscillation technologies beyond the diffraction limit," *Nat. Rev. Phys.* **4**(1), 16–32 (2022).
11. F. M. Huang and N. I. Zheludev, "Super-resolution without evanescent waves," *Nano Lett.* **9**(3), 1249–1254 (2009).
12. K. S. Rogers et al., "Optimising superoscillatory spots for far-field super-resolution imaging," *Opt. Express* **26**(7), 8095–8112 (2018).
13. D. Tang et al., "Ultrabroadband superoscillatory lens composed by plasmonic metasurfaces for subdiffraction light focusing," *Laser Photonics Rev.* **9**(6), 713–719 (2015).
14. Z. Wu et al., "Broadband dielectric metalens for polarization manipulating and superoscillation focusing of visible light," *ACS Photonics* **7**(1), 180–189 (2019).
15. E. T. F. Rogers et al., "A super-oscillatory lens optical microscope for subwavelength imaging," *Nat. Mater.* **11**(5), 432–435 (2012).
16. Y. Yu et al., "An investigation of influencing factors on practical sub-diffraction-limit focusing of planar super-oscillation lenses," *Nanomaterials* **8**(4), 185 (2018).
17. G. H. Yuan, E. T.F. Rogers, and N. I. Zheludev, "Achromatic super-oscillatory lenses with sub-wavelength focusing," *Light: Sci. Appl.* **6**(9), e17036 (2017).
18. J. Diao et al., "Controllable design of super-oscillatory planar lenses for sub-diffraction-limit optical needles," *Opt. Express* **24**(3), 1924–1933 (2016).
19. K. Huang et al., "Optimization-free superoscillatory lens using phase and amplitude masks," *Laser Photonics Rev.* **8**(1), 152–157 (2014).
20. G. H. Yuan et al., "Quantum super-oscillation of a single photon," *Light: Sci. Appl.* **5**(8), e16127 (2016).
21. Q. Zhang et al., "High-numerical-aperture dielectric metalens for super-resolution focusing of oblique incident light," *Adv. Opt. Mater.* **8**(9), 1901885 (2020).
22. F. Qin et al., "A supercritical lens optical label-free microscopy: sub-diffraction resolution and ultra-long working distance," *Adv. Mater.* **29**(8), 1602721 (2017).
23. Z. Duan, H. Chen, and X. Lin, "Optical multi-task learning using multi-wavelength diffractive deep neural networks," *Nanophotonics* **12**(5), 893–903 (2023).
24. H. Chen et al., "Diffractive deep neural networks at visible wavelengths," *Engineering* **7**(10), 1483–1491 (2021).
25. Z. Zheng et al., "Dual adaptive training of photonic neural networks," *Nat. Mach. Intell.* **5**(10), 1119–1129 (2023).
26. T. Zhou et al., "Large-scale neuromorphic optoelectronic computing with a reconfigurable diffractive processing unit," *Nat. Photonics* **15**(5), 367–373 (2021).
27. D. Semwogerere and E. R. Weeks, "Confocal microscopy," *Encyclopedia Biomater. Biomed.l Eng.* **23**, 1–10 (2005).
28. A. D. Elliott, "Confocal microscopy: principles and modern practices," *Curr. Protoc. Cytometry* **92**(1), e68 (2020).
29. M. Gu et al., "Optically digitalized holography: a perspective for all-optical machine learning," *Engineering* **5**(3), 363–365 (2019).
30. S. Lee, C. Park, and J. Rho, "Mapping information and light: trends of AI-enabled metaphotonics," *Curr. Opin. Solid State Mater. Sci.* **29**, 101144 (2024).
31. T. Badloe, S. Lee, and J. Rho, "Computation at the speed of light: metamaterials for all-optical calculations and neural networks," *Adv. Photonics* **4**(6), 064002 (2022).

32. X. Lin et al., "All-optical machine learning using diffractive deep neural networks," *Science* **361**(6406), 1004–1008 (2018).
33. S. Gao et al., "Super-resolution diffractive neural network for all-optical direction of arrival estimation beyond diffraction limits," *Sci. Appl.* **13**(1), 161 (2024).
34. Z. Wang et al., "Opto-intelligence spectrometer using diffractive neural networks," *Nanophotonics* **13**, 3883–3893 (2024).
35. H. Chen and Y. Shen, "Large-scale distributed diffractive-interference hybrid photonic chiplets," *Adv. Photonics* **6**(4), 040502 (2024).

Hang Chen is a postdoctoral researcher and research associate at Tsinghua University. He received his BS, MS, and PhD degrees in the School of Instrumentation Science and Engineering from Harbin Institute of Technology in 2015, 2017, and 2022, respectively. He is the author of more than 20 journal papers. His current research interests include photonic neural networks and integrated photonic chips. He is an editorial board member of *Acta Optica Sinica* and Chinese Laser Press.

Sheng Gao is a PhD student in the Department of Electronic Engineering at Tsinghua University. He received his BE and MS degrees from the School of Information and Electronics, Beijing Institute of Technology, in 2019 and 2022. His current research interests include photonic computing, diffractive neural networks, and electromagnetics.

Haiou Zhang is an engineer in the Department of Electronic Engineering at Tsinghua University. She received her master's degree from Liaoning University in 2017. Her current research interests include photonic computing.

Zejia Zhao is a PhD student in the Department of Electronic Engineering at Tsinghua University. She received her BE degree from the School of Optoelectronic Engineering at Xidian University in 2023. Her current research interests include optical nonlinearity, photonic computing, and metasurfaces.

Zhengyang Duan is a PhD student in the Department of Electronic Engineering at Tsinghua University. He received his BE degree from the Department of Electronic Engineering at Tsinghua University in 2022. His current research interests include the theory, design, and training of optical neural networks and optical-electronic heterogeneous computing architecture.

Gordon Wetzstein is an associate professor of electrical engineering and, by courtesy, of computer science at Stanford University. He is the leader of the Stanford Computational Imaging Lab and a faculty co-director of the Stanford Center for Image Systems Engineering. At the intersection of computer graphics and vision, artificial intelligence, computational optics, and applied vision science, his research has a wide range of applications in next-generation imaging, wearable computing, and neural rendering systems. He is a fellow of Optica and the recipient of numerous awards, including an NSF CAREER Award, an Alfred P. Sloan fellowship, an ACM Siggraph significant new researcher award, a presidential early career award for scientists and engineers (PECASE), an SPIE early career achievement award, an electronic imaging scientist of the year award, an Alain Fournier PhD dissertation award, as well as many best paper and demo awards.

Xing Lin is a tenure-track assistant professor with the Department of Electronic Engineering, Tsinghua University, leading the Tsinghua Photonic Computing and Integration Research Lab. He received his BE degree in electronic engineering from Xidian University in 2010 and his PhD in automation from Tsinghua University in 2015. He was a research associate with Stanford University from 2015 to 2017, a postdoctoral scholar with the University of California, Los Angeles, from 2017 to 2019, and a research scientist with Beijing-Tsinghua Innovation Center for Future Chips from 2019 to 2021. His research interests include photonic computing, optical neural networks, and neuromorphic photonics. He was the recipient of MIT TR35 Asia Pacific, AI Chinese Young Scholar, and the Science and Technology Progress Award (first prize) of the Chinese Institute of Electronics.